Bioorganic Chemistry 111 (2021) 104897

Contents lists available at ScienceDirect

Bioorganic Chemistry

journal homepage: www.elsevier.com/locate/bioorg

# Inverse Virtual Screening for the rapid re-evaluation of the presumed biological safe profile of natural products. The case of steviol from *Stevia rebaudiana* glycosides on farnesoid X receptor (FXR)

Marianna Potenza [a], Maria Maddalena Cavalluzzi [b], Gualtiero Milani [b], Gianluigi Lauro [a], Adriana Carino [c], Rosalinda Roselli [d], Stefano Fiorucci [c], Angela Zampella [d], Ciro Leonardo Pierri [e], Giovanni Lentini [b], Giuseppe Bifulco [a,*]

[a] Department of Pharmacy, University of Salerno, Via Giovanni Paolo II 132, Fisciano 84084, Italy
[b] Department of Pharmacy – Drug Sciences, University of Bari Aldo Moro, Via Edoardo Orabona, 4, Bari 70126, Italy
[c] Department of Surgery and Biomedical Sciences, Nuova facoltà di Medicina, Perugia, Italy
[d] Department of Pharmacy, University of Naples, Via Domenico Montesano, 49, Naples 80131, Italy
[e] Department of Biosciences, Biotechnologies, and Biopharmaceutics, University of Bari Aldo Moro, Via Edoardo Orabona, 4, Bari 70126, Italy

ARTICLE INFO

*Keywords:*
Inverse virtual screening
Natural products
Molecular docking
Target identification
Farnesoid X receptor

ABSTRACT

Nonnutritive sweeteners (NNSs) are widely employed as dietary substitutes for classical sugars thanks to their safety profile and low toxicity. In this study, a re-evaluation of the biological effects of steviol (**1**), the main metabolite from *Stevia rebaudiana* glycosides, was performed using the Inverse Virtual Screening (IVS) target fishing computational approach. Starting from well-known pharmacological properties of *Stevia rebaudiana* glycosides, this computational tool was employed for predicting the putative interacting targets of **1** and, afterwards, of its five synthetic ester derivatives **2**–**6**, accounting a large panel of proteins involved in cancer and inflammation events. Applying this methodology, the farnesoid X receptor (FXR) was identified as the putative target partner of **1**–**6**. The predicted ligand-protein interactions were corroborated by transactivation assays, specifically disclosing the agonistic activity of **1** and the antagonistic activities of **2**–**6** on FXR. The reported results highlight the feasibility of IVS as a fast and potent tool for predicting the interacting targets of query compounds, addressing the re-evaluation of their bioactivity. In light of the obtained results, the presumably safe profile of known compounds, such as the case of steviol (**1**), is critically discussed.

## 1. Introduction

Polypharmacology represents an emerging concept in the field of natural products [1] and drug discovery. Many studies were reported regarding potent and originally selective compounds, able to accomplish the "one target, one drug" paradigm, but later re-evaluated for their activities on additional macromolecules [2]. The rational design of multi-target-based compounds still represents a challenge for the scientific community, and novel, fast, and accurate computational methods are even more required with this aim [3]. In the last decade, remarkable efforts were made by different research groups in order to develop robust computational protocols and tools for accelerating the target identification of organic compounds (i.e., TarFisDock [4], PharmMapper [5], Pocketome [6], BioGPS [7]). With this aim, we implemented a new computational approach named Inverse Virtual Screening (IVS) [8,9], introducing the normalization of the predicted binding affinities as the key parameter for the target selection. Afterwards, this methodology was widely applied for successfully predicting and validating the interacting targets of bioactive compounds from both natural and synthetic sources [10–13]. In details, case–study compounds (both natural or synthesized ones) are tested through molecular docking experiments against panels of protein targets, usually collected for their involvement in specific pathologies, and preferred ligand-protein interactions are quickly predicted from an in silico evaluation. This approach could also be useful for repositioning synthetic molecules initially designed for specific targets [13] as well as for facilitating the discovery of multi-target binders [12]. In the field of natural products, IVS represents a potent tool when the bioactivity of a compound is known (e.g.

* Corresponding author.
*E-mail address:* bifulco@unisa.it (G. Bifulco).

https://doi.org/10.1016/j.bioorg.2021.104897
Received 7 August 2020; Received in revised form 20 January 2021; Accepted 5 April 2021
Available online 8 April 2021

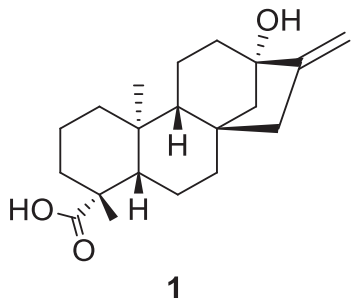


1

**Fig. 1.** Steroid-like chemical structure of steviol (**1**).

anticancer, anti-inflammatory, antiviral, etc.) but its interacting targets are unknown, thus providing relevant information to clarify the observed pharmacological action. Furthermore, IVS can be applied for the discovery of potential off-targets for compounds whose targets of interaction are already known, then aiding to clarify possible undesired effects of the case-study compounds. Thus, this approach can be also proficiently used to interrogate the presumed safe profile of a bioactive compound. This is particularly important for re-evaluating approved drugs or in the case of natural compounds, for which a rapid prediction of additional targets of interaction could call into question their supposed safety.

In this study, we examined this latter aspect showing the application of the IVS approach on natural products and, specifically, investigating steviol (compound **1**, Fig. 1) as case-study compound. This molecule represents the colonic metabolite of the glycosides found in leaves of *Stevia rebaudiana* Bertoni, a nonnutritive sweetener (NNS) and sugar substitute, due to the steviol glycosides extreme sweetness, with its safety being previously widely reported [14]. Additionally, five steviol derivatives (compounds **2**–**6**, Fig. 6) were evaluated for deeper investigations and for evaluating the possible modulation of the biological activities on a small set of structurally related compounds.

## 2. Materials and methods

### 2.1. Inverse Virtual Screening

The chemical structures of the investigated compounds (**1–6**) (see Results and Discussion) were built with Maestro Build Panel (Schrödinger, LLC, New York, NY, 2017) [15]. For each case-study molecule (compounds **1**–**6**), different "blank" compounds, used for the normalization of the predicted binding affinities (*vide infra*), were selected featuring similar chemical features of the query compounds. Prior to performing molecular docking calculations, optimizations (Conjugate Gradient, 0.05 Å convergence threshold) of the structures were applied to identify possible three-dimensional starting geometries. Then, all the structures were converted in the pdbqt format using OpenBabel software (version 2.3.2), adding Gasteiger charges.

312 Protein 3D structures were prepared by downloading the PDB files from the Protein Data Bank database (www.rcsb.org). Details about the panel of proteins are reported in Table S1 (Supporting Information).

Molecular docking calculations were performed using the Autodock-Vina software [16]. In the configuration files linked to the 3D structures of the proteins, coordinates and dimensions along x, y, z-axes of the grid related to the site of presumable pharmacological interest, with a spacing of 1.0 Å between the grid points, were reported. The exhaustiveness value was set to 64, saving 10 conformations as a maximum number of binding modes. For all the investigated compounds, all open-chain bonds were treated as active torsional bonds.

A group of promising interacting proteins of **1**–**6** was selected, setting a predicted binding affinity cutoff = −7.5 kcal/mol. For each compound, the identified proteins were then also accounted for further molecular docking rounds against "blank" molecules, the latter needed for the normalization of the binding affinities of the investigated compounds, as reported in the following equation:

$$V = V_0/V_R$$

where, for each investigated target, V represents the normalized value of the investigated compounds **1**–**6**, $V_0$ is its predicted binding affinity from docking calculations (kcal/mol) for the investigated compound, $V_R$ is the average value of binding energy calculated on all the "blanks" (kcal/mol). It is important to note that V is a dimensionless number, and then it can be used to predict the interacting targets of a case-study compound rather than to have precise indications about the related binding affinities. After the normalization process, a final ranking was obtained, from the most to the least promising target. Normalized values and predicted binding energies for the selected targets of **1**–**6** are collected in Tables S2–S7 (Supporting Information), respectively. Then, for each selected target, the obtained docking poses of **1**–**6** were compared with the 3D structure of the co-crystallized ligand, when available, by computing the shape similarity parameter using Phase software [15] (Tables S2–S7, Supporting Information). In particular, "in place" shape similarity was computed, namely skipping the conformational sampling of the screened compounds, since the conformers considered were those already sampled and arising from the molecular docking calculations. The ligand/protein complexes were visually inspected with Maestro.

### 2.2. Molecular dynamics simulations

The docking poses of **1** and **5** were used as input for two molecular dynamics simulation rounds on FXR protein, using Desmond software [17]. The starting complexes were prepared with the System Builder in Desmond, setting a cubic box with a 10 Å buffer distance and the TIP3P water model for solvation and OPLS-2005 force field, adding $Na^+$ ions for obtaining the electroneutrality. The built systems were then minimized by LBFGS method, setting a maximum number of 2000 iterations and a convergence threshold of 1.0 kcal/mol/Å. Then, the minimized systems were submitted to the following relaxation protocol: 1) NVT simulation at 10 K (1 ns), with solute non-hydrogen atoms restrained; 2) NVT simulation (120 ps), using the Berendsen thermostat at 10 K, with fast temperature relaxation constant, a velocity resampling every 1 ps and non-hydrogen solute atoms restrained; 3) NPT simulation (120 ps), using the Berendsen thermostat and the Berendsen barostat at 10 K, setting a pressure of 1 atm (fast temperature relaxation constant, a slow pressure relaxation constant, velocity resampling every 1 ps, non-hydrogen solute atoms restrained); 4) NPT ensemble simulation (120 ps), using the Berendsen thermostat and the Berendsen barostatat 300 K and 1 atm, with a fast temperature relaxation constant, a slow pressure relaxation constant, velocity resampling every 1 ps and non-hydrogen solute atoms restrained; 5) NPT simulation (240 ps), using the Berendsen thermostat and the Berendsen barostatat 300 K and 1 atm, with a fast temperature relaxation constant and a normal pressure relaxation constant. Eventually, MD simulations of 100 ns at 310 K, using a recording interval of 1.2 ps and an NPT ensemble class (1.01 bar) were performed, setting 2.0 fs as integration timestep.

### 2.3. General synthetic procedures

Rebaudioside A was purchased as a commercial sweetener (Farmalabor, Italy). All reagents were purchased from Sigma–Aldrich or Alfa Aesar at the highest quality commercially available. Solvents were RP grade unless otherwise indicated. Yields refer to purified products and were not optimized. The structures of the compounds were confirmed by routine spectrometric and spectroscopic analyses. Only spectra for compounds not previously described are given. Melting points were determined on a Gallenkamp apparatus in open glass capillary tubes and are uncorrected. Infrared spectra were recorded on a Perkin–Elmer (Norwalk, CT) Spectrum One FT spectrophotometer and band positions

are given in reciprocal centimeters ($cm^{-1}$). $^1H$ and $^{13}C$ NMR spectra were recorded on a Varian Mercury-VX spectrometer (Varian Inc., Palo Alto, CA, USA), operating at 300 and 75 MHz for $^1H$ and $^{13}C$, respectively, or on a Agilent Technologies 500 MHz (Varian Inc., Palo Alto, CA, USA), operating at 500 and 125 MHz for $^1H$ and $^{13}C$, respectively, using $CDCl_3$ as a solvent. Chemical shifts are reported in parts per million (ppm) relative to the residual non-deuterated solvent resonance: $CDCl_3$, $\delta$ 7.26 ($^1H$ NMR) and $\delta$ 77.3 ($^{13}C$ NMR). *J* values are given in Hz. HRMS analyses were performed using a Bruker microTOF QII mass spectrometer equipped with ESI operating in both positive and negative ion mode. Elemental analyses were performed with a Eurovector Euro EA 3000 analyzer. Optical rotations were measured on a Perkin Elmer (Norwalk, CT) Mod 341 spectropolarimeter; concentrations are expressed in g/100 mL, and the cell length was 1 dm, thus $[\alpha]^{20}{}_D$ values are given in units of $10^{-1}$ deg $cm^2$ $g^{-1}$. Chromatographic separations were performed on silica gel columns by flash chromatography (Kieselgel 60, 0.040–0.063 mm, Merck, Darmstadt, Germany). TLC analyses were performed on precoated silica gel on aluminum sheets (Kieselgel 60 F254, Merck).

Steviol (**1**) was prepared as reported in the literature [18,19]. Spectrometric and spectroscopic data were in agreement with the previously reported ones [20].

#### 2.3.1. Synthesis of steviol benzyl ester (2)

The procedure adopted for the synthesis of steviol benzyl ester (**2**) is described. A solution of steviol (**1**) (0.170 g, 0.53 mmol), benzyl bromide (0.110 g, 0.64 mmol) and $K_2CO_3$ (0.149 g, 1.08 mmol) in 4 mL of abs EtOH was stirred at 90 °C for 11 min in a microwave reactor. After evaporation of the solvent, the residue was taken up with EtOAc, in turn washed with 1 M NaOH and brine. The organic phase, dried over anhydrous $Na_2SO_4$ and evaporated under vacuum, gave 0.208 g of a yellow solid which was recrystallized from MeOH to give 0.138 g of the desired product (63%): mp 156–158 °C (MeOH); $[\alpha]_D^{20}$ = –74.9 (*c* 2, $CHCl_3$); IR (KBr): 3485 (OH), 1700 (C═O) $cm^{-1}$; $^1H$ NMR ($CDCl_3$,500 MHz): $\delta$ 0.77 (3H, s overlapping dt at 0.80), 0.80 (1H, dt overlapping s at 0.77, *J* = 13.7, 4.4 Hz), 0.94 (1H, d, *J* = 8.3 Hz), 0.99 (1H, dt overlapping dd at 1.05, *J* = 13.2, 4.4 Hz), 1.05 (1H, dd overlapping dt at 0.99, *J* = 12.0, 2.2 Hz), 1.19 (3H, s), 1.22 (1H, dd, *J* = 10.8, 2.0 Hz), 1.36–1.46 (2H, m), 1.50–1.64 (4H, m), 1.70–1.78 (3H, m), 1.78–1.90 (3H, m), 2.02–2.08 (2H, m), 2.14–2.18 (1H, m), 2.20 (1H, bd, *J* = 14.7 Hz), 4.80 (1H, s), 4.96 (1H, s), 5.02 (1H, d, *J* = 12.2 Hz), 5.13 (1H, d, *J* = 12.2 Hz), 7.30–7.40 (5H, m); $^{13}C$ NMR ($CDCl_3$, 125 MHz): $\delta$ 15.4 , 19.1 , 20.4, 21.9, 28.8, 38.0, 39.2, 39.3, 40.7, 41.3, 41.6, 43.9, 46.9, 47.4, 53.7, 57.1, 66.0, 80.2, 102.9, 128.1, 128.2 (2C), 128.5 (2C), 136.1, 156.1, 177.2; HRMS *m/z* 431.2556 $[M+Na]^+$ (calcd for $C_{27}H_{36}O_3$: 431.2557 $[M+Na]^+$); anal. C, 77.84; H, 8.58%, calcd for $C_{27}H_{36}O_3{\cdot}0.5H_2O$: C, 77.66; H, 8.93%.

#### 2.3.2. Synthesis of steviol 4-iodobenzyl ester (3)

The title compound was prepared from steviol (**1**) and 4-iodobenzyl bromide in 72% yield as a yellowish solid: mp 148–150 °C; $[\alpha]_D^{20}$ = –53.7 (*c* 2, $CHCl_3$); IR (KBr): 3493 (OH), 1704 (C═O) $cm^{-1}$; $^1H$ NMR ($CDCl_3$, 500 MHz): $\delta$ 0.76 (3H, s overlapping m at 0.76–0.84), 0.76–0.84 (1H, m overlapping s at 0.76), 0.94 (1H, d, *J* = 7.8 Hz), 1.00 (1H, dt overlapping d at 1.05, *J* = 14.0, 4.2 Hz), 1.05 (1H, d overlapping dt at 1.00, *J* = 12.0 Hz), 1.18 (3H, s), 1.24 (1H, d, *J* = 11.2 Hz), 1.36–1.46 (2H, m), 1.48–1.68 (4H, m), 1.70–1.78 (3H, m), 1.78–1.86 (3H, m), 2.02 (1H, d overlapping d at 2.05, *J* = 11.5 Hz), 2.05 (1H, d overlapping d at 2.02, *J* = 17.6 Hz), 2.18 (2H, bd, *J* = 16.5 Hz), 4.80 (1H, s), 4.94 (1H, d, *J* = 13.0 Hz), 4.97 (1H, s), 5.08 (1H, d, *J* = 13.0 Hz), 7.10 (2H, d, *J* = 8.3 Hz), 7.69 (2H, d, *J* = 8.3 Hz); $^{13}C$ NMR ($CDCl_3$, 125 MHz): $\delta$ 15.5, 19.0, 20.4, 21.9, 28.8, 38.0, 39.2, 39.3, 40.6, 41.3, 41.6, 43.9, 47.0, 47.4, 53.7, 57.0, 65.3, 80.2, 93.7, 102.9, 130.1 (2C), 135.7, 137.6 (2C), 156.0, 177.0; HRMS *m/z* 557.1520 $[M+Na]^+$ (calcd for $C_{27}H_{35}IO_3$: 557.1523 $[M+Na]^+$); anal. C, 59.63; H, 6.43%, calcd for $C_{27}H_{35}IO_3{\cdot}0.5H_2O$: C, 59.67; H, 6.68%.

#### 2.3.3. Synthesis of steviol 2-(3,5-di-tert-butyl-4-hydroxyphenyl)-2-oxoethyl ester (4)

The title compound was prepared from steviol (**1**) and 2-bromo-3′-5′-di-*tert*-butyl-4′-hydroxy acetophenone in 63% yield as a colorless oil: $[\alpha]_D^{20}$ = –49.3 (*c* 2, $CHCl_3$); $^1H$ NMR ($CDCl_3$, 500 MHz): $\delta$ 0.82 (1H, b dt, *J* = 13.1, 4.1 Hz), 0.91 (3H, s), 0.97 (1H, d, *J* = 8.0 Hz), 1.04 (1H, dt overlapping m at 1.06–1.10, *J* = 13.5, 4.2 Hz), 1.06–1.10 (1H, m overlapping dt at 1.04), 1.26 (1H, dd, *J* = 13.0, 2.0 Hz), 1.31 (3H, s), 1.38–1.48 (1H, m overlapping s at 1.44), 1.44 (18H, s overlapping m at 1.38–1.48), 1.48–1.64 (3H, m), 1.72–1.80 (4H, m), 1.82–1.96 (4H, m), 2.06 (1H, dd, *J* = 17.0, 2.0 Hz), 2.14 (1H, dd overlapping dt at 2.18, *J* = 11.2, 2.8 Hz), 2.18 (1H, dt overlapping dd at 2.14, *J* = 17.0, 2.8 Hz), 2.27 (1H, bd, *J* = 13.5 Hz), 4.80 (1H, s), 4.96 (1H, s), 5.18 (1H, d, *J* = 16.1 Hz), 5.38 (1H, d, *J* = 16.1 Hz), 5.70 (1H, s), 7.78 (2H, s); $^{13}C$ NMR ($CDCl_3$, 125 MHz): $\delta$ 14.2, 15.8, 19.1, 20.4, 21.0, 21.8, 29.0, 30.1 (6C), 34.4, 38.1, 39.2, 39.4, 40.7, 41.4, 41.6, 44.1, 47.0, 47.4, 53.8, 57.0, 60.4, 65.1, 80.2, 102.8, 125.5, 126.3, 136.1, 156.2, 158.9, 177.0, 191.6; HRMS *m/z* 563.3733 $[M^-]$.(calcd for $C_{36}H_{51}O_5$: 563.3742 $[M^-]$).

#### 2.3.4. Synthesis of steviol 2,3-dichlorobenzyl ester (5)

The title compound was prepared from steviol (**1**) and 2,3-dichlorobenzyl bromide in 78% yield as a white solid: mp 188–190 °C (MeOH); $[\alpha]_D^{20}$ = –49.9 (*c* 2, $CHCl_3$); IR (KBr): 3500 (OH), 1700 (C═O) $cm^{-1}$; $^1H$ NMR ($CDCl_3$, 300 MHz): $\delta$ 0.76 (3H, s overlapping dt at 0.80), 0.80 (1H, dt overlapping s at 0.76, *J* = 12.9, 4.1 Hz), 0.90–1.10 (3H, m), 1.21 (3H, s overlapping m at 1.22–1.30), 1.22–1.30 (1H, m overlapping s at 1.21), 1.34–1.92 (12H, m), 1.96–2.10 (2H, m), 2.10–2.26 (2H, m), 4.79 (1H, s), 4.96 (1H, s), 5.10 (1H, d, *J* = 12.9 Hz), 5.25 (1H, d, *J* = 12.9 Hz), 7.20 (1H, t, *J* = 7.9 Hz), 7.35 (1H, dd, *J* = 7.6, 1.8 Hz), 7.40 (1H, dd, *J* = 8.2, 1.8 Hz); $^{13}C$ NMR ($CDCl_3$, 75 MHz): $\delta$ 15.4, 19.0, 20.4, 21.8, 28.8, 38.0, 39.2, 39.3, 40.6, 41.3, 41.6, 44.0, 46.9, 47.4, 53.7, 57.0, 63.8, 80.2, 102.9, 127.3, 128.2, 130.2, 132.1, 133.3, 136.1, 156.0, 177.0; HRMS *m/z* 499.1794 $[M+Na]^+$ (calcd for $C_{27}H_{34}Cl_2O_3$: 499.1777 ($[M+Na]^+$); anal. C, 65.74; H, 6.87%, calcd for $C_{27}H_{34}Cl_2O_3{\cdot}0.75H_2O$: C, 66.05; H, 7.29%.

#### 2.3.5. Synthesis of steviol 4-nitrobenzyl ester (6)

The title compound was prepared from steviol (**1**) and 4-nitrobenzyl bromide in 55% yield as a yellow solid: mp 170–172 °C (EtOAc/hexane); $[\alpha]_D^{20}$ = –48.8 (*c* 2, $CHCl_3$); IR (KBr): 3497 (OH), 1707 (C═O) $cm^{-1}$; $^1H$ NMR ($CDCl_3$, 500 MHz): $\delta$ 0.79 (3H, s overlapping dt at 0.82), 0.82 (1H, dt overlapping s at 0.79, *J* = 13.7, 3.8 Hz), 0.96 (1H, d, *J* = 8.3 Hz), 1.04 (1H, dt overlapping dd at 1.09, *J* = 14.3, 4.8 Hz), 1.09 (1H, dd overlapping dt at 1.04, *J* = 12.0, 1.7 Hz), 1.21 (3H, s overlapping dd at 1.24), 1.24 (1H, dd overlapping s at 1.21, *J* = 7.5, 2.5 Hz), 1.38–1.66 (6H, m), 1.68–1.90 (6H, m), 2.03 (1H, dd overlapping dd at 2.06, *J* = 11.0, 2.5 Hz), 2.06 (1H, dd overlapping dd at 2.03, *J* = 18.0, 1.5 Hz), 2.16–2.24 (2H, m), 4.80 (1H, s), 4.96 (1H, s), 5.07 (1H, d, *J* = 13.7 Hz), 5.25 (1H, d, *J* = 13.7 Hz), 7.52 (2H, d, *J* = 8.3 Hz), 8.23 (2H, d, *J* = 8.3 Hz); $^{13}C$ NMR ($CDCl_3$, 125 MHz): $\delta$ 15.5, 19.0, 20.4, 21.9, 28.8, 38.0, 39.2, 39.3, 40.5, 41.2, 41.6, 44.0, 46.9, 47.3, 53.7, 56.9, 64.6, 80.2, 103.0, 123.8 (2C), 128.5 (2C), 143.4, 147.6, 155.9, 176.9; HRMS *m/z* 476.2408 ($[M+Na]^+$ (calcd for $C_{27}H_{35}NO_5$: 476.2407 $[M+Na]^+$); anal. C, 69.98; N, 3.28; H, 7.73%, calcd for $C_{27}H_{35}NO_5{\cdot}0.5H_2O$: C, 70.10; N, 3.03; H, 7.84%.

### 2.4. Cell culture

HepG2, a human immortalized hepatocarcinoma cell line, was cultured and maintained at 37 °C and 5% $CO_2$ in E-MEM additioned with 10% FBS, 1% glutamine and 1% penicillin/streptomycin.

### 2.5. Transactivation assay

To evaluate FXR mediated transactivation, HepG2 cells were transfected with 100 ng of human pSG5-FXR, 100 ng of human pSG5-RXR, 200 ng of the reporter vector p(hsp27)-TK-LUC containing the FXR

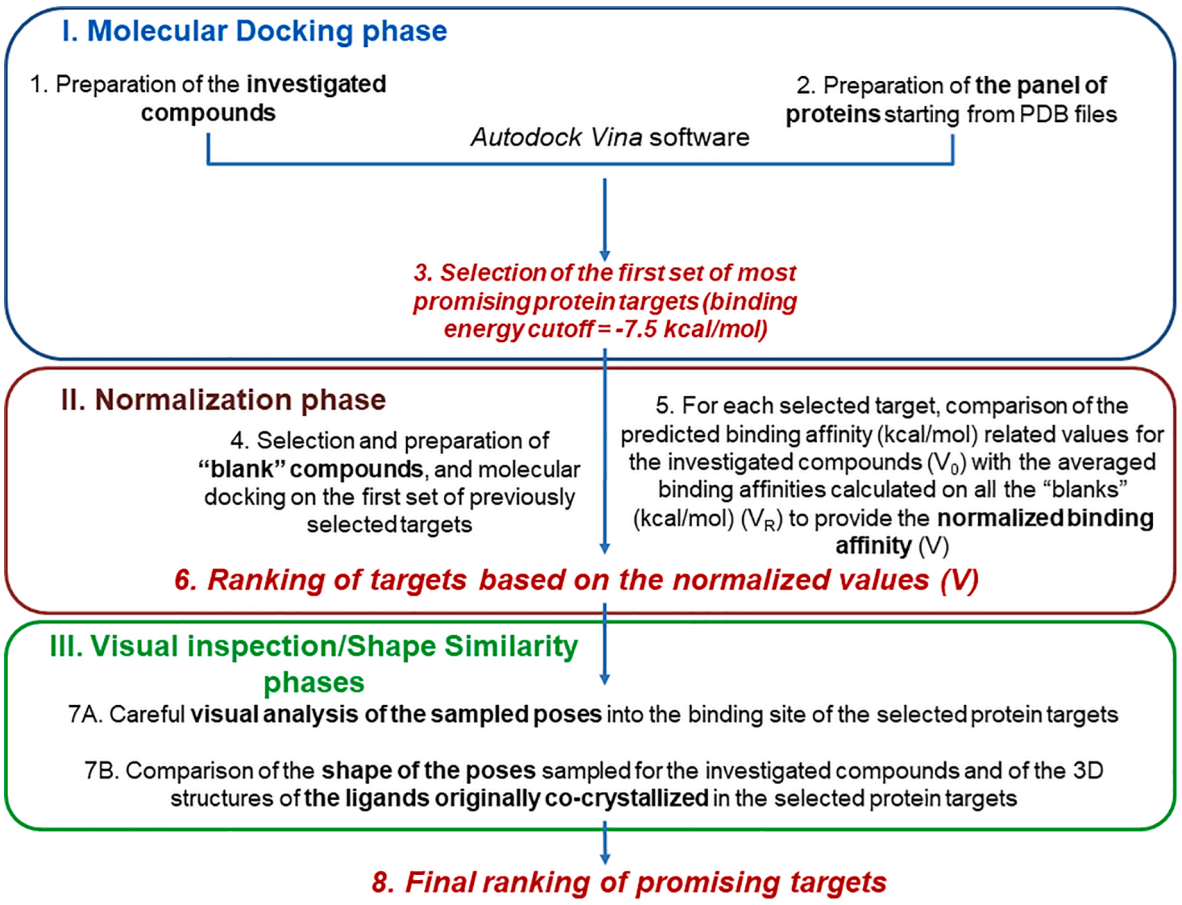


**Fig. 2.** Inverse Virtual Screening (IVS) workflow.

response element IR1 cloned from the promoter of heat shock protein 27 (hsp27) and with 100 ng of pGL4.70 (Promega), a vector encoding the human Renilla gene. At 24 h post-transfection, cells were stimulated 18 h with CDCA and compounds **1**–**6** (10 and 50 μM). In another experimental setting, at 24 h post-transfection, cells were stimulated with 50 μM of compounds in combination with CDCA (10 μM). After treatments, 10 μL of cellular lysates were read using a Dual-Luciferase Reporter Assay System (Promega Italia srl, Milan, Italy) according manufacturer specifications using the Glomax20/20 luminometer (Promega Italia srl, Milan, Italy). Luciferase activities were assayed and normalized with Renilla activities.

### 2.6. Dose–response curve on FXR

To calculate the activity of compound **1** (steviol) and of its derivatives **3** and **5** on FXR, dose response curves were performed in HepG2 cells transfected as described above and then treated with increasing concentrations of compounds **1** (from 0.1 to 100 μM) alone or in combination with CDCA (10 μM), and compounds **3** and **5** in combination with CDCA. At 18 h post stimulations, cellular lysates were assayed for luciferase and Renilla activities using the Dual-Luciferase Reporter Assay System (E1980, Promega Italia srl, Milan, Italy). Luminescence was measured using Glomax 20/20 luminometer (Promega Iralia srl, Milan, Italy). Luciferase activities were normalized with Renilla activities. The potency of tested compounds was expressed as $EC_{50}$ or $IC_{50}$.

### 2.7. Statistical analysis

Statistical analysis were performed with Prism 6.0 software (GraphPad). The non parametric Mann–Whitney *U* test was used for statistical comparisons (*p < 0.05 vs NT cells, #p < 0.05 vs CDCA treated cells).

## 3. Results and discussion

### 3.1. Computational studies performed on steviol (1)

In this study, novel interacting targets of steviol (**1**, Fig. 1) were predicted and validated employing the Inverse Virtual Screening (IVS) computational approach. The IVS workflow followed in this study is reported in Fig. 2. Briefly, molecular docking experiments (Autodock-Vina software) [16] were performed using **1** as the case-study compound to be tested against a large panel of protein targets involved in the progression of tumor and inflammatory diseases (312 items).

After setting a predicted binding energy cutoff of −7.5 kcal/mol, 19 targets were roughly selected (see Table S2, Supporting Information). Afterwards, applying a normalization of the binding affinity [8,9] values for **1** against each selected protein (see Materials and Methods), the most promising macromolecules were ranked from the highest to the lowest normalized value (defined as V, see Materials and Methods) and they were further selected considering the following filters:

- visual inspection analysis of the binding mode of the ligand within the ligand-binding site;
- superimposition between the ligand and the co-crystallized binders, when the latter were available. This analysis was based on the "shape similarity" parameter, which indicates the comparison between two chemical species through a comparison of their 3D shapes, and it can numerically range from 0 (no one atom matching) to 1 (all atoms matching showing the same conformational arrangment) (see Table S2, Supporting Information).

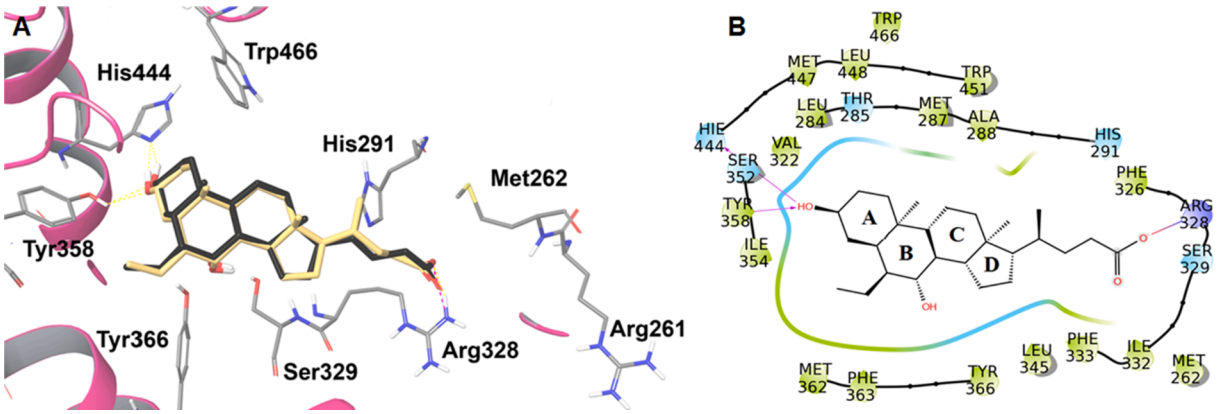


**Fig. 3.** A) Superimposition between 6-ECDCA binding mode deriving from docking experiments (in yellow) and co-crystallized 6-ECDCA (black) onto the ligand binding site of the chain A of the crystal structure of FXR (PDB code: 1OSV); chain A is depicted in purple ribbons, and key residues in the binding site of FXR are represented in sticks, C grey, N blue, O red, S yellow, polar H white; H-bonds and salt bridges are reported as dotted yellow and purple lines, respectively. B) 2D diagram interactions of 6-ECDCA with the key residues in the binding site of chain A of the crystal structure of FXR (PDB code: 1OSV); positive charged, polar and hydrophobic residues are colored in blue, in light blue, and in green respectively; H-bonds are reported as violet arrows; A, B, C, D ring names are assigned in the structure representation. (For interpretation of the references to color in this figure legend, the reader is referred to the web version of this article.)

According to IVS analysis, farnesoid X receptor (FXR) was predicted as the most promising protein target of **1** (See Table S2, Supporting Information), since it showed the highest V value (see Materials and Methods) among the investigated targets in the panel, thus locating at the top of the protein ranking. In order to corroborate the efficiency of the applied computational approach and to further confirm the obtained result, accurate investigations of the binding poses of **1** onto the FXR binding site were performed while also evaluating their superimposition with the FXR co-crystallized ligand [21] 6-ethylchenodeoxycholic acid (6-ECDCA) [22] (PDB code: 1OSV), against which steviol showed a shape similarity value = 0.39.

Specifically, bile acids (BAs) and other well-known steroid-like

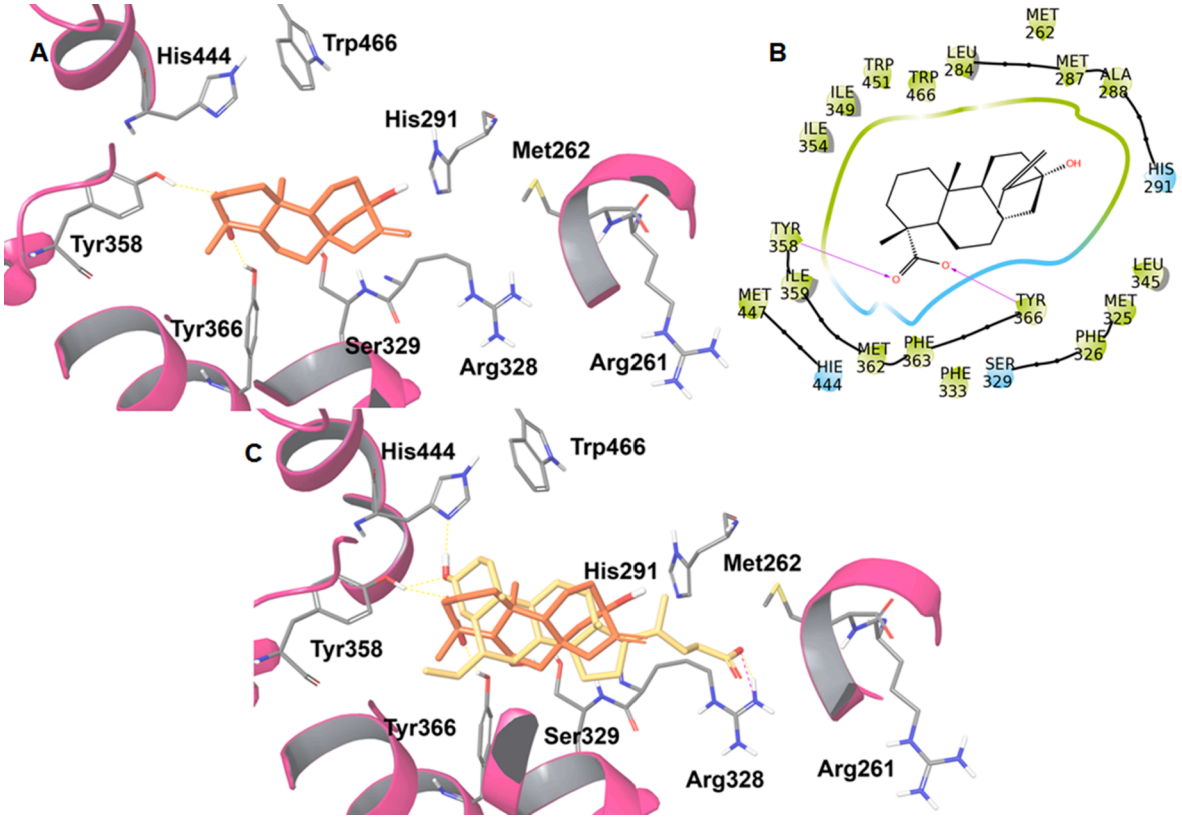


**Fig. 4.** A) 3D representation of steviol **1** (in orange) onto the binding site of the chain A of the crystal structure of FXR (PDB code: 1OSV); chain A is depicted in purple ribbons, and key residues in the binding site of FXR are represented in sticks, C grey, N blue, O red, S yellow, polar H white; H-bonds are reported as dotted yellow lines. B) 2D diagram interactions of steviol **1** with the key residues in the binding site of chain A of the crystal structure of FXR (PDB code: 1OSV); positive charged, polar and hydrophobic residues are colored in blue, in light blue, and in green, respectively; H-bonds are reported as violet arrows. C) 3D superimposition of 6-ECDCA (in yellow) and steviol **1** (in orange) onto the binding site of the chain A of the crystal structure of FXR (PDB code: 1OSV); chain A is depicted in purple ribbons, and key residues in the binding site of FXR are represented in sticks, C grey, N blue, O red, S yellow, polar H white; H-bonds and salt bridges are reported as dotted yellow and purple lines, respectively. (For interpretation of the references to color in this figure legend, the reader is referred to the web version of this article.)

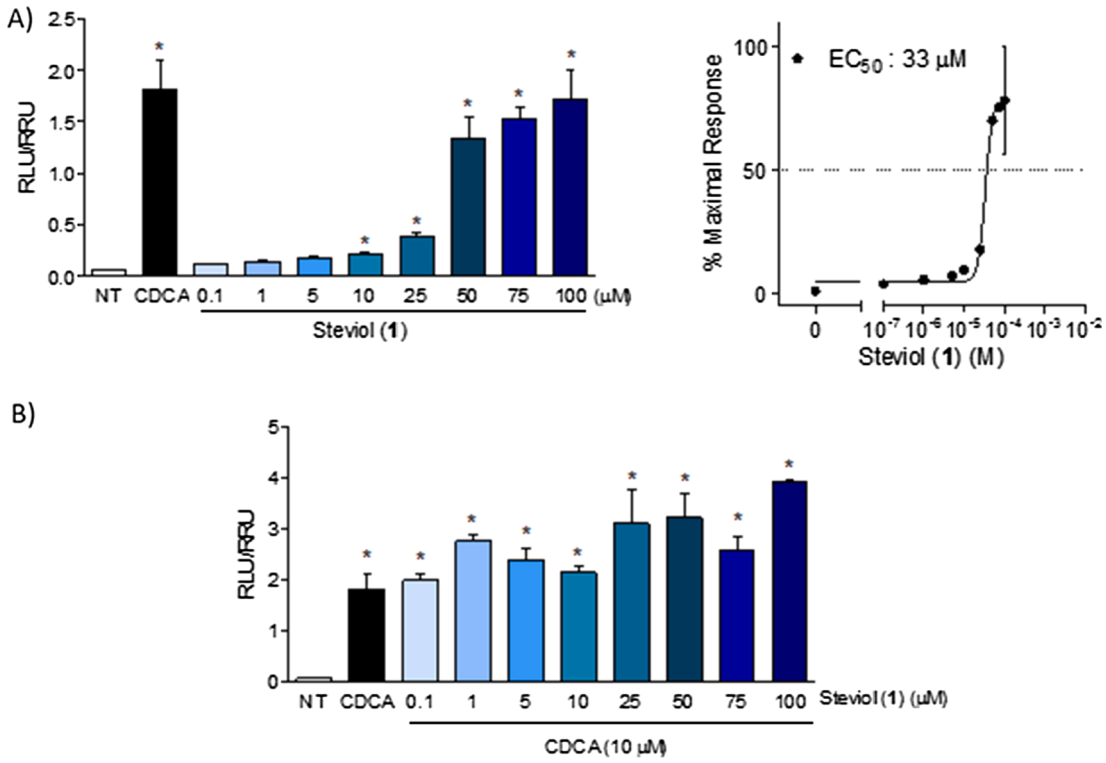


**Fig. 5.** HepG2 cells were transfected with FXR as described above and used in a luciferase reporter assay. Twenty-four hours post transfection cells were stimulated with increasing concentrations of compound 1 range from 100 nM to 100 μM alone or in combination with CDCA 10 μM. Concentration-response curves to evaluate A) agonism and B) antagonism for FXR on compound **1**. Results are expressed as mean ± standard error. *p < 0.05 vs NT cells.

agonists [21,23] of FXR receptor are generally amphiphilic molecules characterized by a concave hydrophilic *β*-face and a convex lipophilic *α*-face [21,24]. The classical nuclear receptor (NR) fold consists of 12 helices forming a three-layer sandwich hosting the ligand-binding site. Specifically, ligand binding of agonists induces a rearrangement to the active conformation of both the loop H1-H2 and helix H12 at the same time, promoting the recruitment of co-activator proteins [24]. In light of this, the simultaneous interaction of a binder with Tyr358 of helix 11 and Met262 of the loop H1-H2 leads to the agonism versus the receptor [24]. As a reference, the analysis of the key interactions exerted by the investigated compounds with the receptor counterpart was performed taking into account the binding mode of the co-crystallized 6-ethylchenodeoxycholic acid (6-ECDCA) (PDB code: 1OSV) [21].

Firstly, 6-ECDCA was re-docked onto the ligand binding site of FXR Autodock-Vina experiments, in order to verify whether the chosen computational parameters (see Materials and Methods) were able to reproduce the experimental binding mode [21], obtaining satisfactory outcomes (Fig. 3). Furthermore, the accurate analysis of the ligand-protein complex highlighted His444 on helix 10/11 and Trp466 on helix 12 as the two residues involved in the receptor activation trigger. The A ring and the 3α-hydroxy group of the ligand were oriented toward helix 12, interacting with His444 and with Tyr358, thus inducing the formation of a π-cation interaction between the indole ring of Trp466 and the Nε of the His444. This interaction cannot be established in the absence of ligand, as the physical constraints on these residues are not optimal [21] (Fig. 3). The hydrogen bonds between the carboxylate oxygens of the ligand and both Met262 of the loop H1-H2 and Arg328 of helix 5 were other essential interactions since, together with Arg287, His291 and Phe333, they form a channel responsible for the entrance of the agonists to the canonical binding site when helix 12 is in the active conformation, and which connects the latter to a noncanonical binding site of antagonists.

The visual inspection of the sampled poses disclosed steviol (**1**) as a ligand able to establish a set of key interactions with the receptor counterpart (Fig. 4). On the other hand, it is important to note that the reduced volume of **1** caused a limited set of interactions onto the binding site if compared to those established by 6-ECDCA. Specifically, the carboxyl group of **1** was oriented towards helix 12, H-bonding with Tyr358 and Tyr366, thus placing at the same region occupied from the ring system of 6-ECDCA (Fig. 4). Also, a weak interaction with His291 by means of the hydroxyl group was detected. According to this analysis, steviol (**1**) accomplished a wide set of key interactions with the receptor counterpart, supporting the hypothesized favorable binding to FXR. Also, molecular dynamics simulations performed on the FXR/**1** complex (100 ns) provided interesting details about the putative agonistic activity of the investigated compound. Indeed, the analysis of this simulation disclosed that the π-cation interaction between His444 and Trp466 is not affected by the binding of **1**, as clearly indicated by the plot of the distances between these two hotspot residues along the whole simulation (See Fig. S1a, Supporting Information). Also, the plot of the root-mean square deviation (RMSD, Å) related to the protein backbone confirmed the structure stability of the complex during such simulation (see Fig. S1b, Supporting Information), thus pointing out steviol (**1**) being unable to induce remarkable conformational changes to the protein and supporting its putative FXR agonistic activity. Taken together, all these considerations corroborated the IVS preliminary indications, thus highlighting nuclear Farnesoid X Receptor (FXR) as a promising target of **1**.

### 3.2. *In vitro evaluation of the activity of steviol on FXR*

To further investigate the preliminary results, we evaluated the activity of steviol (**1**) on FXR in a transactivation assay on HepG2 cells transiently transfected with human FXR. As reference compound, CDCA was used in concentrations of 10 μM. As shown in Fig. 5, steviol transactivated FXR in a concentration-dependent manner with an $EC_{50}$ of 33 μM (Fig. 5A, *p < 0.05 vs NT cells), whereas it did not show antagonistic activity, rather enhancing the effect of CDCA at increasing

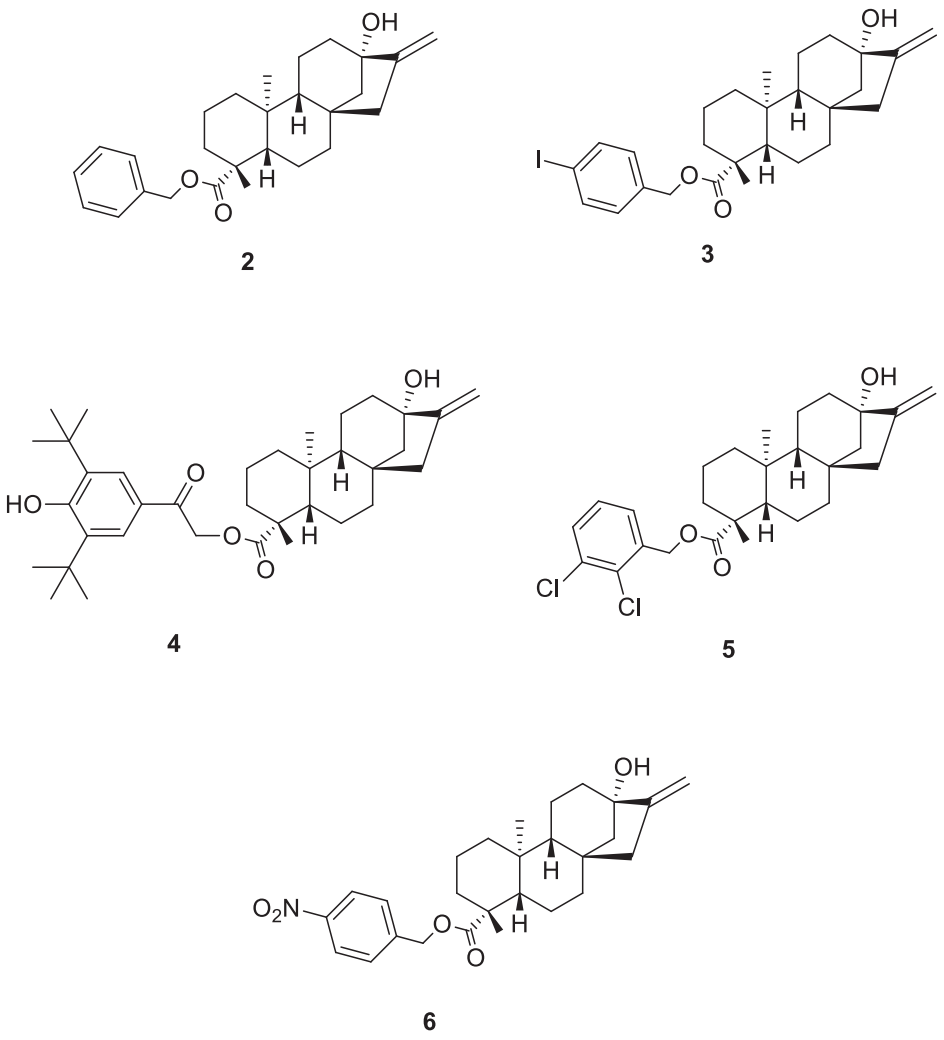


**Fig. 6.** Chemical structures of steviol derivatives **2–6**.

concentrations (Fig. 5B, *p < 0.05 vs NT cells).

This biological result corroborated the computational predictions, thus enforcing the reliability of IVS in the field of the target prediction. The moderate activity found for this natural product is in line with the hypothesis of its modulatory role and is consistent with a controlled exposure to a renowned non-toxic agent (i.e., food product). On the other hand, the interference of steviol with FXR activity suggested a critical discussion of its presumed safety, especially when it could be used in high doses.

Indeed, FXR is a nuclear hormone receptor expressed in the liver and gut and it is a master regulator of the synthesis and pleiotropic actions of endogenous bile acids (BAs) acting as ligands. In general, it regulates many genes involved in lipid and glucose metabolism, liver regeneration, inflammation, and liver cancer [25]. In particular, the activation of FXR reduces circulating bile acids (feedback mechanism) and it participates in the regulation of lipids and glucose homeostasis in the gut-liver axis, controlling glucose metabolism through the regulation of gluconeogenesis and glycogenolysis in the liver and of peripheral insulin sensitivity in striated muscle and adipose tissue. Importantly, FXR agonists have proven effective in reducing steatohepatitis in non alcoholic fatty liver disease (NAFLD) and non-alcoholic steatohepatitis (NASH) patients [26]. In patients with NASH [26] the expression of FXR is downregulated, whereas these levels are inversely correlated with disease severity. Furthermore, FXR activation protects against hepatic steatosis by reducing lipogenesis and promoting fatty acid β-oxidation [27]. Thus, FXR is generally involved in the maintenance of energy homeostasis and the functionality of several organs. In light of the last considerations, the use of steviol (**1**) in diabetic patients as substituent of the classical sugar is encouraged. However, the activation of FXR could cause side effects too, considering the systemic effects versus a large variety of tissues in the whole body. Indeed, in possible particular pathological conditions, the general energy status as well as tissue specificity are important factors to be accounted after FXR activation. This suggests that the outcomes of this activation should be carefully evaluated [28]. Additionally, elevated levels of cholesterol in plasma were observed in the evaluation of the effects of the agonist 6-ECDCA in clinical trials, probably related to the total inhibition of BAs biosynthesis from cholesterol [29]. In light of all the considerations above and basing on IVS outcomes, we questioned the safe profile of steviol (**1**). On the other hand, the inhibition of FXR leads to some positive outcomes in dysmetabolic diseases and, for these reasons, we took into account the possibility of modulating the agonistic activity of steviol (**1**) on FXR receptor towards an antagonistic activity introducing some modifications on its chemical structure.

### 3.3. *Generation of steviol derivatives (**2–6**)*

Starting from these preliminary computational results, we also wondered whether simple chemical modifications on the steviol scaffold could modulate its pharmacological activity on FXR. Indeed, simple variations on FXR agonist chemotypes could lead to a shift of the activity possibly leading to the transition from the agonist to the antagonist

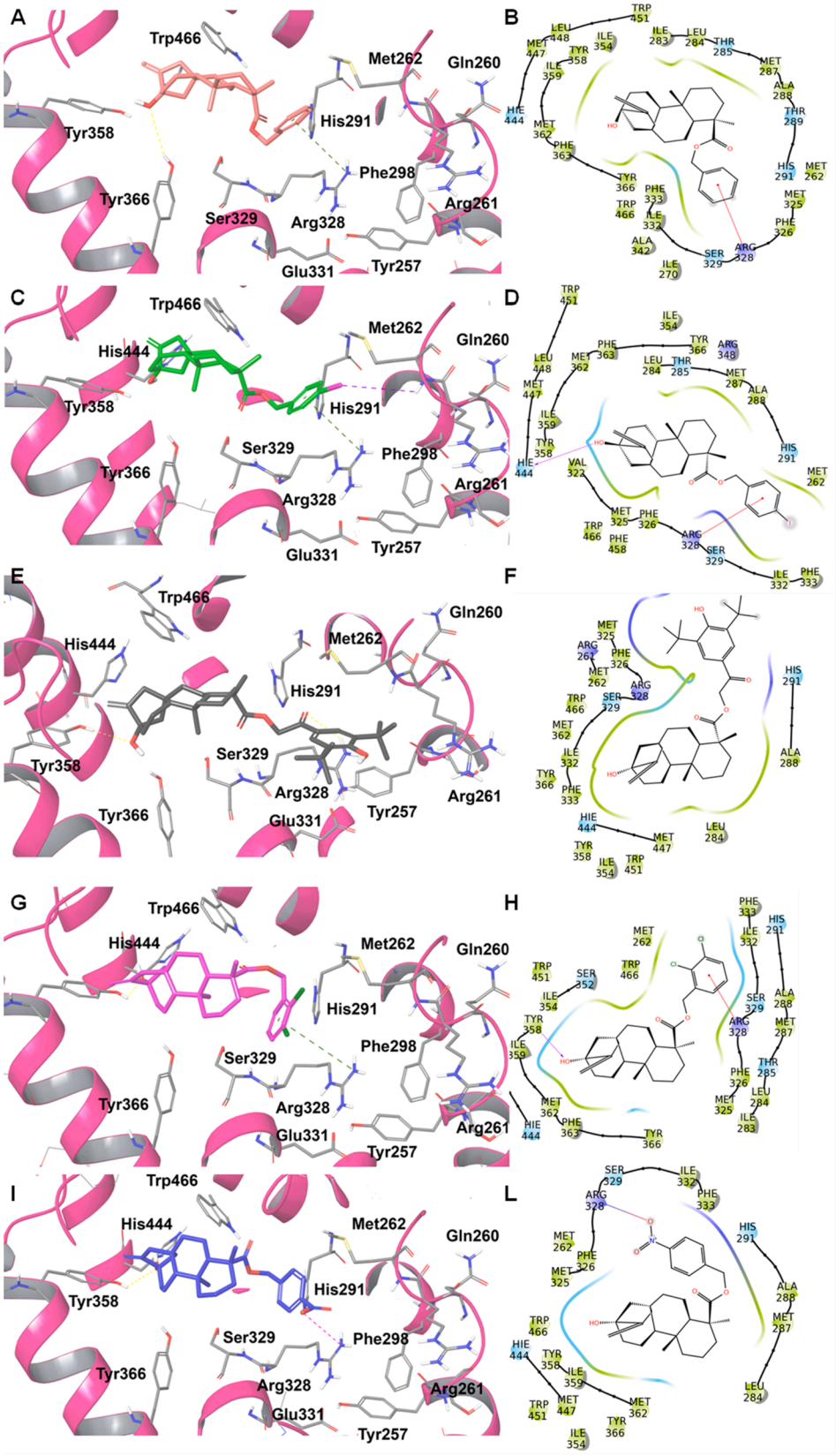


**Fig. 7.** On the left, 3D representation of compounds **2** (colored by atom types: C pink, O red, polar H white), **3** (colored by atom types: C light green, O red, I violet, polar H white), **4** (colored by atom types: C dark grey, O red, polar H white), **5** (colored by atom types: C violet, O red, Cl green, polar H white), and **6** (colored by atom types: C blue, O red, N blue, polar H white) onto the binding site of the chain A of the crystal structure of FXR (PDB code: 1OSV), with chain A depicted in purple ribbons; key residues in the binding site of FXR are represented in sticks, C grey, N blue, O red, S yellow, polar H white; H-bonds interactions are depicted in yellow dotted lines, π-π interactions in green dotted lines, and halogen bonds in violet dotted lines. On the right, 2D diagram interactions of compounds **2**, **3**, **4**, **5** and **6** with the key residues in the binding site of chain A of the crystal structure of FXR (PDB code: 1OSV); positive charged, polar and hydrophobic residues are colored in violet, in light blue, and in green, respectively; H-bonds are reported as violet arrows, while π-π and π-cation interactions as green and red lines, respectively. (For interpretation of the references to color in this figure legend, the reader is referred to the web version of this article.)

profile [30], the latter aimed for the treatment of dysmetabolic syndromes [31]. In this scenario, it is also important to highlight that FXR antagonists could be as well structurally similar in size to well-known FXR agonists [32–35], and in this case their antagonistic activity is mainly based on their different chemical features influencing the sets of interaction with the receptor counterpart or on their ability of exploring different regions in the ligand binding site. Starting from steviol, we tested its analogues **2**–**6** (Fig. 6) by means of molecular docking

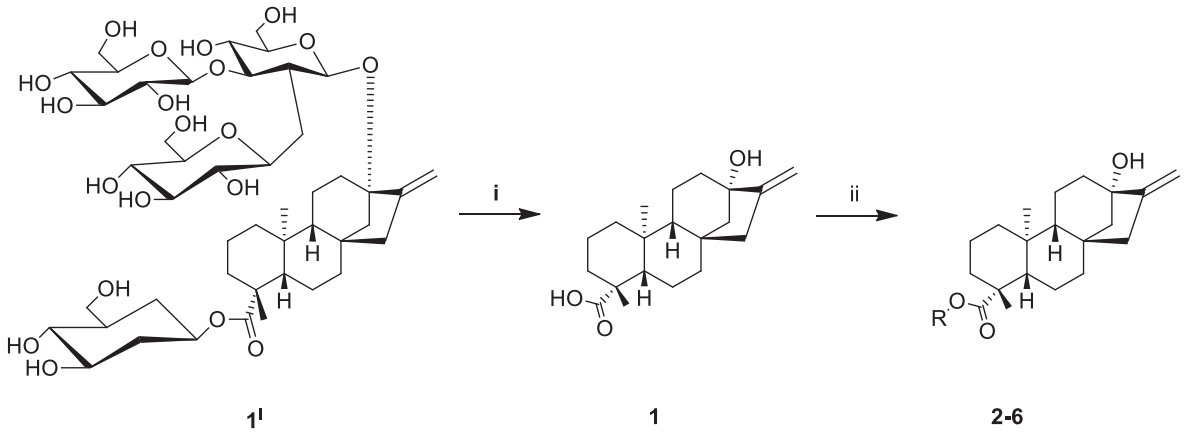


**Scheme 1.** Synthesis of steviol derivatives **2–6**[a]. [a]Reagents and conditions: i) $NaIO_4$, $H_2O$, rt, 96 h; then KOH, 100 °C, 1 h; ii) R–Br (benzyl or phenacyl bromide), $K_2CO_3$, abs EtOH, microwave irradiation, 90 °C, 11 min.

experiments. In this case, we wondered whether the introduction of steric hindrance could trigger a transition from the agonism of steviol (**1**) to antagonism in derivatives **2–6**, considering the hypothesis that the increase of the volume could be the key chemical feature for the modulation of the activity. In this context, a benzyl ester moiety could be easily introduced at the carboxyl group position (**2**), while variously decorated electron-deficient (as for compounds **3**, **5**, **6**) and electron-rich bulky aromatic substituents (as for compound **4**) could be accounted as well (see Chemistry section). Preliminary docking experiments were performed on steviol derivatives **2–6** onto the ligand-binding site of chain A of the 3D structure of FXR (PDB: 1OSV) [21], in order to support their putative binding to FXR at a molecular level. Furthermore, in order to corroborate such supposed interactions, IVS experiments were also applied to compound **2–6**, screening them against the panel of 312 protein previously accounted for steviol (**1**). In the final normalized ranking related to compounds **2–6**, FXR was again found among the top positions of the related rankings, thus confirming it as a possible preferred target of interaction (see Tables S3–S8, Supporting information).

Firstly, if compared with cognate agonists, FXR antagonists are often more voluminous, and this chemical feature is mainly responsible of the destabilization of the receptor active conformation. Also, from a computational point of view, FXR antagonism can be obtained when the query compound is not able to simultaneously interact with Tyr358 and Met262. Finally, the ability of the compounds of binding to a non canonical binding site placed between the loop region H1-H2, helix 3, helix 5 and helix 8 is another aspect to be investigated, since it is generally considered as a valuable computational hypothesis concerning the FXR antagonism field. Starting from these premises, the accurate analysis of the docking poses related to compounds **2–6** highlighted their putative FXR antagonistic activity. Indeed, all the compounds showed a good superimposition with the co-crystallized ligand, placing their steroid-like skeleton at the center of the pocket while exploring a further region of the receptor with the aromatic ring of the ester moiety. On the other hand, the hydroxyl group of compound **6** established hydrogen bonds with His444 and Tyr358, whereas the interaction between its nitro group and Arg328 forced the ligand so that no interactions with Met262 were detectable. Compounds **2**, **3**, and **5** were able to establish a π-cation interaction between Arg328 and the aromatic ring of the ester as well as hydrogen bonds with His444 and Tyr358 by means of the hydroxyl group on the other side, showing a binding mode similar to those of compounds **6**. Furthermore, a specific halogen bond interaction with Arg261 was detected for compounds **3** (see Fig. 7). Considering compound **4**, it was able to interact with Tyr358 by means of the hydroxyl group, while its carbonyl group was involved in hydrogen bond interaction with Arg328, forcing its steric hindrance towards the side of the entrance to the binding site (Fig. 7).

**Table 1**
List of bromides used in the synthesis of compounds 2–6.

| Compound | Benzyl or phenacyl bromide |
|---|---|
| **2** | 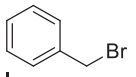 |
| **3** | 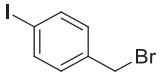 |
| **4** | 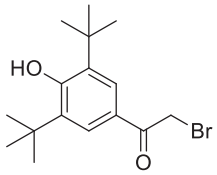 |
| **5** | 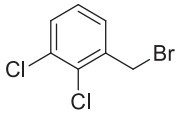 |
| **6** | 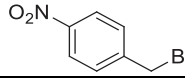 |

Since molecular docking experiments indicated the ability of **2–6** in establishing a different pattern of interactions if compared with those established by steviol (**1**), molecular dynamics simulations (100 ns) were performed, specifically accounting FXR/**5** as representative system to be investigated and to be possibly compared with FXR/**1** complex (*vide supra*). Also in this case, the analysis of this simulation was focused on analyzing the plot of the distances between His444 and Trp466 (See Fig. S2a, Supporting Information), in order to assess whether the π-cation interaction between these two key residues could be affected by the ligand binding. Remarkably, we noticed high fluctuations of the distance between His444 and Trp466 along the simulation (See Fig. S2a, Supporting Information), indicating the possible ability of steviol derivatives in interfering with this key interaction, as also confirmed by the visual inspection of the trajectory frames. Also, the analysis of the protein backbone root-mean square deviation (RMSD, Å) plot indicated, differently from what observed for FXR/**1** complex, more evident fluctuations in the protein architecture (See Fig. S2b, Supporting Information). All together, these investigations at molecular level pointed out steviol derivatives **2–6** as putative FXR binders endowed with antagonistic activity.

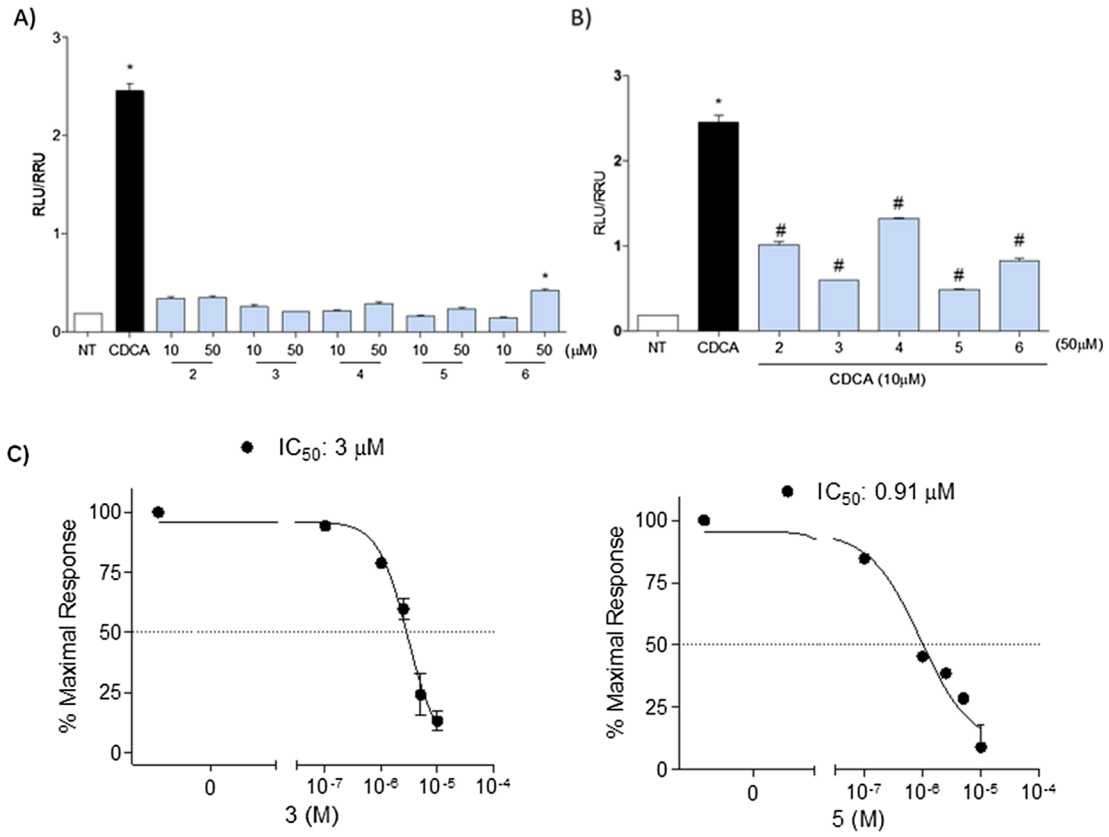


**Fig. 8.** A) HepG2 FXR/RXR agonism evaluation on compounds **2**–**6**; B) HepG2 FXR/RXR antagonism evaluation on compounds **2**–**6**; C) Concentration-response curves of compounds **3** and **5** to evaluate their antagonistic activity on FXR. *p < 0.05 vs NT cells; #p < 0.05 vs CDCA treated cells.

### *3.4. Chemistry*

Steviol (**1**) and its derivatives **2**–**6** were obtained as depicted in Scheme 1. Steviol (**1**) was obtained from Rebaudioside A (**1**[I]) by an oxidative alkaline hydrolysis procedure developed on the basis of two previously reported methods, which started from stevioside [18] and rebaudioside A [19], respectively. The obtained compound **1** was then reacted with the respective benzyl or phenacyl bromide [36] (Table 1) under microwave irradiation to afford the desired compounds (**2**–**6**).

### *3.5. In vitro evaluation of the activity of steviol derivatives **2**–**6** on FXR*

Given the preliminary results, we investigated the activity of steviol derivatives **2**–**6** on FXR in HepG2 cells transiently transfected with human FXR. We found that none of the tested compounds showed agonistic activity on FXR (Fig. 8A, *p < 0.05 vs NT cells). Conversely, our results indicated that all steviol derivatives (**2**–**6**) showed a FXR antagonistic activity when tested in combination with CDCA, used as reference agonist (Fig. 8B, *p < 0.05 vs NT cells; #p < 0.05 vs CDCA treated cells). In detail, compounds **3** and **5** presented the strongest antagonistic activity, whereas compound **4** showed a lower antagonism on FXR in comparison to its structural cognates. Thus, we investigated the relative potency of the most promising compounds **3** and **5**, by a detailed measurement of concentration-response curve in trans-activation assay on HepG2 cells. As illustrated in Fig. 8C, both compounds **3** and **5** inhibited the FXR transactivation in a concentration-dependent manner with an $IC_{50}$ of 3.0 and 0.91 μM respectively, showing a stronger antagonistic activity in comparison to the well-known FXR antagonist Guggulsterone [37,38], whose $IC_{50}$ value is 15 μM.

As mentioned above, the inhibition of FXR leads to some positive outcomes in specific diseases. The reduction of the activity of the receptor, in fact, induces an increase of the catabolism of cholesterol from the liver, which is converted in bile acids, reducing this way the levels of cholesterol in plasma. Considering that the lower explored field of FXR antagonism may be a new and encouraging strategy for the treatment of dysmetabolic diseases, the novel steviol derivatives **2**–**6**, quickly identified as novel FXR antagonists, may be considered as a starting point for further chemical and biological investigations.

## 4. Conclusions

The application of the IVS computational approach for the discovery of the residual activities of natural compounds, affecting their presumed biological safe profile, was here reported. This methodology led to the fast prediction of the interacting targets of steviol (**1**), disclosing its agonism on FXR. The possible effects on FXR agonism were critically discussed, thus questioning the presumed safe profile of steviol (**1**). Also, simple structural modifications were introduced on steviol with the purpose of modulating its agonism on the nuclear FXR, leading to the identification of a novel class of FXR antagonists (compounds **2**–**6**), possibly useful for the treatment of dysmetabolic diseases. The biological experiments on the novel steviol derivatives **2**–**6** showed their antagonistic activity on FXR, with compound **3** and **5** exhibiting an $IC_{50}$ value of 3.0 and 0.91 μM, respectively. The identification of the interacting targets and the elucidation of the biological activity of steviol, consequently applied for the discovery of a novel class of pharmacologically active compounds, highlighted IVS as a robust tool for quickly investigating the biological profile of presumably safe natural compounds. Also, molecular docking-based IVS methodology combined with further comprehesive computational approaches, such as molecular dynamics, represent a valuable toolkit for predicting the different biological behaviors of structurally related compounds (e.g., the modulation of the agonist/antagonist activity). The application of this

methodology can be rapidly re-iterated on large sets of natural products, suggesting its use for rapid biological screenings and for orienting the specific pharmacological investigations, while also accelerating the development of new classes of nature-inspired compounds for the treatment of specific pathologies.

## Declaration of Competing Interest

The authors declare that they have no known competing financial interests or personal relationships that could have appeared to influence the work reported in this paper.

## Acknowledgement

G. B. acknowledges the financial support of MIUR Italy PRIN 2017 project (2017A95NCJ) "Stolen molecules – Stealing natural products from the depot and reselling them as new drug candidates" and a 2014 to 2020 POR CAMPANIA FESR grant from the Regional Council of Campania Region, entitled "Campania OncoTerapie - Combattere la resistenza tumorale: piattaforma integrata multidisciplinare per un approccio tecnologico"

## Appendix A. Supplementary material

Information about the panel of 312 targets used in this study, the final rankings of predicted interacting targets for compounds **1-6** and details about MD simulations are available free of charge *via* the Internet at. Supplementary data to this article can be found online at https://doi.org/10.1016/j.bioorg.2021.104897.

## References

[1] J. Fang, C. Liu, Q. Wang, P. Lin, F. Cheng, In silico polypharmacology of natural products, Brief. Bioinform. 19 (2018) 1153–1171, https://doi.org/10.1093/bib/bbx045.
[2] B.M. Kuenzi, L.L. Remsing Rix, P.A. Stewart, B. Fang, F. Kinose, A.T. Bryant, T. A. Boyle, J.M. Koomen, E.B. Haura, U. Rix, Polypharmacology-based ceritinib repurposing using integrated functional proteomics, Nat. Chem. Biol. 13 (12) (2017) 1222–1231, https://doi.org/10.1038/nchembio.2489.
[3] R.R. Ramsay, M.R. Popovic-Nikolic, K. Nikolic, E. Uliassi, M.L. Bolognesi, A perspective on multi-target drug discovery and design for complex diseases, Clin. Transl. Med. 7 (2018) 3, https://doi.org/10.1186/s40169-017-0181-2.
[4] H. Li, Z. Gao, L. Kang, H. Zhang, K. Yang, K. Yu, X. Luo, W. Zhu, K. Chen, J. Shen, X. Wang, H. Jiang, TarFisDock: a web server for identifying drug targets with docking approach, Nucleic Acids Res. 34 (Web Server) (2006) W219–W224, https://doi.org/10.1093/nar/gkl114.
[5] X. Wang, Y. Shen, S. Wang, S. Li, W. Zhang, X. Liu, L. Lai, J. Pei, H. Li, PharmMapper 2017 update: a web server for potential drug target identification with a comprehensive target pharmacophore database, Nucleic Acids Res. 45 (2017) W356–W360, https://doi.org/10.1093/nar/gkx374.
[6] I. Kufareva, A.V. Ilatovskiy, R. Abagyan, Pocketome: an encyclopedia of small-molecule binding sites in 4D, Nucl. Acids Res. 40 (2011) D535–D540, https://doi.org/10.1093/nar/gkr825.
[7] L. Siragusa, S. Cross, M. Baroni, L. Goracci, G. Cruciani, BioGPS: Navigating biological space to predict polypharmacology, off-targeting, and selectivity, Proteins Struct. Funct. Bioinf. 83 (2015) 517–532, https://doi.org/10.1002/prot.24753.
[8] Simona De Vita, Gianluigi Lauro, Dafne Ruggiero, Stefania Terracciano, Raffaele Riccio, Giuseppe Bifulco, Protein Preparation Automatic Protocol for High-Throughput Inverse Virtual Screening: Accelerating the Target Identification by Computational Methods, J. Chem. Inf. Model. 59 (11) (2019) 4678–4690, https://doi.org/10.1021/acs.jcim.9b00428.
[9] Gianluigi Lauro, Adriana Romano, Raffaele Riccio, Giuseppe Bifulco, Inverse Virtual Screening of Antitumor Targets: Pilot Study on a Small Database of Natural Bioactive Compounds, J. Nat. Prod. 74 (6) (2011) 1401–1407, https://doi.org/10.1021/np100935s.
[10] Gianluigi Lauro, Milena Masullo, Sonia Piacente, Raffaele Riccio, Giuseppe Bifulco, Inverse Virtual Screening allows the discovery of the biological activity of natural compounds, Bioorg. Med. Chem. 20 (11) (2012) 3596–3602, https://doi.org/10.1016/j.bmc.2012.03.072.
[11] M.C. Proto, D. Fiore, C. Piscopo, S. Franceschelli, V. Bizzarro, C. Laezza, G. Lauro, A. Feoli, A. Tosco, G. Bifulco, G. Sbardella, M. Bifulco, P. Gazzerro, Inhibition of Wnt/beta-Catenin pathway and Histone acetyltransferase activity by Rimonabant: a therapeutic target for colon cancer, Sci. Rep. 7 (2017) 11678, https://doi.org/10.1038/s41598-017-11688-x.
[12] C. Ostacolo, V. Di Sarno, G. Lauro, G. Pepe, S. Musella, T. Ciaglia, V. Vestuto, G. Autore, G. Bifulco, S. Marzocco, P. Campiglia, I.M. Gomez-Monterrey, A. Bertamino, Identification of an indol-based multi-target kinase inhibitor through phenotype screening and target fishing using inverse virtual screening approach, Eur. J. Med. Chem. 167 (2019) 61–75, https://doi.org/10.1016/j.ejmech.2019.01.066.
[13] Mario Scrima, Gianluigi Lauro, Manuela Grimaldi, Sara Di Marino, Alessandra Tosco, Paola Picardi, Patrizia Gazzerro, Raffaele Riccio, Ettore Novellino, Maurizio Bifulco, Giuseppe Bifulco, Anna Maria D'Ursi, Structural evidence of N6-isopentenyladenosine as a new ligand of farnesyl pyrophosphate synthase, J. Med. Chem. 57 (18) (2014) 7798–7803, https://doi.org/10.1021/jm500869x.
[14] Amir Abbas Momtazi-Borojeni, Seyed-Alireza Esmaeili, Elham Abdollahi, Amirhossein Sahebkar, A Review on the Pharmacology and Toxicology of Steviol Glycosides Extracted from Stevia rebaudiana, Curr. Pharm. Des. 23 (11) (2017) 1616–1622, https://doi.org/10.2174/1381612822666161021142835.
[15] Schrödinger LLC., Maestro, version 11.1.012; Phase, version 5.0; Schrödinger LLC: New York, NY, USA, 2017.
[16] O. Trott, A.J. Olson, AutoDock Vina: improving the speed and accuracy of docking with a new scoring function, efficient optimization, and multithreading, J. Comput. Chem. 31 (2010) 455–461, https://doi.org/10.1002/jcc.21334.
[17] Desmond Molecular Dynamics System, D.E. Shaw Research, New York, NY, 2017.
[18] Tomoya Ogawa, Michio Nozaki, Masanao Matsui, Total synthesis of stevioside, Tetrahedron 36 (18) (1980) 2641–2648, https://doi.org/10.1016/0040-4020(80)80136-0.
[19] R.N. Khaibullin, I.Yu. Strobykina, V.E. Kataev, O.A. Lodochnikova, A. T. Gubaidullin, R.Z. Musin, New synthesis of diterpenoid (16S)-dihydrosteviol, Russ. J. Gen. Chem. 79 (5) (2009) 967–971, https://doi.org/10.1134/S107036320905017X.
[20] J.G. Napolitano, C. Simmler, J.B. McAlpine, D.C. Lankin, S.-N. Chen, G.F. Pauli, Digital NMR Profiles as Building Blocks: Assembling 1H Fingerprints of Steviol Glycosides, J. Nat. Prod. 78 (2015) 658–665, https://doi.org/10.1021/np5008203.
[21] Li-Zhi Mi, Srikripa Devarakonda, Joel M. Harp, Qing Han, Roberto Pellicciari, Timothy M. Willson, Sepideh Khorasanizadeh, Fraydoon Rastinejad, Structural basis for bile acid binding and activation of the nuclear receptor FXR, Mol. Cell 11 (4) (2003) 1093–1100, https://doi.org/10.1016/S1097-2765(03)00112-6.
[22] Roberto Pellicciari, Stefano Fiorucci, Emidio Camaioni, Carlo Clerici, Gabriele Costantino, Patrick R. Maloney, Antonio Morelli, Derek J. Parks, Timothy M. Willson, 6α-Ethyl-Chenodeoxycholic Acid (6-ECDCA), a Potent and Selective FXR Agonist Endowed with Anticholestatic Activity, J. Med. Chem. 45 (17) (2002) 3569–3572, https://doi.org/10.1021/jm025529g.
[23] S.M. Soisson, G. Parthasarathy, A.D. Adams, S. Sahoo, A. Sitlani, C. Sparrow, J. Cui, J.W. Becker, Identification of a potent synthetic FXR agonist with an unexpected mode of binding and activation, Proc. Natl. Acad. Sci. U. S. A. 105 (14) (2008) 5337–5342, https://doi.org/10.1073/pnas.0710981105.
[24] L. Yang, D. Broderick, Y. Jiang, V. Hsu, C.S. Maier, Conformational dynamics of human FXR-RXR ligand interactions studied by hydrogen/deuterium exchange mass spectrometry: insights into the antagonism of the hypolipidemic agent Z-guggulsterone, BBA 2014 (1844) 1684–1693, https://doi.org/10.1016/j.bbapap.2014.06.007.
[25] S. Modica, S. Murzilli, L. Salvatore, D.R. Schmidt, A. Moschetta, Nuclear bile acids receptor FXR protects against intestinal tumorigenesis, Cancer. Res. 68 (2008) 9589–9594, https://doi.org/10.1158/0008-5472.can-08-1791.
[26] S. Fiorucci, M. Biagioli, E. Distrutti, Future trends in the treatment of non-alcoholic steatohepatitis, Pharmacol. Res. 134 (2018) 289–298, https://doi.org/10.1016/j.phrs.2018.07.014.
[27] A. Carino, S. Marchiano, M. Biagioli, C. Fiorucci, A. Zampella, M.C. Monti, E. Moretta, M. Bordoni, C. Di Giorgio, R. Roselli, P. Ricci, E. Distrutti, S. Fiorucci, Transcriptome Analysis of Dual FXR and GPBAR1 Agonism in Rodent Model of NASH Reveals Modulation of Lipid Droplets Formation, Nutrients 11 (2019) 1132, https://doi.org/10.3390/nu11051132.
[28] C.Y. Han, Update on FXR Biology: Promising Therapeutic Target? Int. J. Mol. Sci. 19 (2018) 2069, https://doi.org/10.3390/ijms19072069.
[29] D. Merk, S. Sreeramulu, D. Kudlinzki, K. Saxena, V. Linhard, S.L. Gande, F. Hiller, C. Lamers, E. Nilsson, A. Aagaard, L. Wissler, N. Dekker, K. Bamberg, M. Schubert-Zsilavecz, H. Schwalbe, Molecular tuning of farnesoid X receptor partial agonism, Nat. Commun. 10 (2019) 2915, https://doi.org/10.1038/s41467-019-10853-2.
[30] H. Huang, P. Si, L. Wang, Y. Xu, X. Xu, J. Zhu, H. Jiang, W. Li, L. Chen, J. Li, Design, Synthesis, and Biological Evaluation of Novel Nonsteroidal Farnesoid X Receptor (FXR) Antagonists: Molecular Basis of FXR Antagonism, ChemMedChem 10 (2015) 1184–1199, https://doi.org/10.1002/cmdc.201500136.
[31] S. Modica, A. Moschetta, Nuclear bile acid receptor FXR as pharmacological target: Are we there yet? FEBS Lett. 580 (2006) 5492–5499, https://doi.org/10.1016/j.febslet.2006.07.082.
[32] Carmen Festa, Claudia Finamore, Silvia Marchianò, Francesco Saverio Di Leva, Adriana Carino, Maria Chiara Monti, Federica del Gaudio, Sara Ceccacci, Vittorio Limongelli, Angela Zampella, Stefano Fiorucci, Simona De Marino, Investigation around the Oxadiazole Core in the Discovery of a New Chemotype of Potent and Selective FXR Antagonists, ACS Med. Chem. Lett. 10 (4) (2019) 504–510, https://doi.org/10.1021/acsmedchemlett.8b00534.
[33] Francesco Saverio Di Leva, Carmen Festa, Claudio D'Amore, Simona De Marino, Barbara Renga, Maria Valeria D'Auria, Ettore Novellino, Vittorio Limongelli, Angela Zampella, Stefano Fiorucci, Binding Mechanism of the Farnesoid X Receptor Marine Antagonist Suvanine Reveals a Strategy To Forestall Drug Modulation on Nuclear Receptors. Design, Synthesis, and Biological Evaluation of

Novel Ligands, J. Med. Chem. 56 (11) (2013) 4701–4717, https://doi.org/10.1021/jm400419e.
[34] Valentina Sepe, Eleonora Distrutti, Stefano Fiorucci, Angela Zampella, Farnesoid X receptor modulators 2011–2014: a patent review, Expert Opin. Ther. Pat. 25 (8) (2015) 885–896, https://doi.org/10.1517/13543776.2015.1045413.
[35] Valentina Sepe, Eleonora Distrutti, Stefano Fiorucci, Angela Zampella, Farnesoid X receptor modulators 2014-present: a patent review, Expert Opin. Ther. Pat. 28 (5) (2018) 351–364, https://doi.org/10.1080/13543776.2018.1459569.
[36] Alessia Carocci, Alessia Catalano, Francesco Turi, Angelo Lovece, Maria M. Cavalluzzi, Claudio Bruno, Nicola A. Colabufo, Marialessandra Contino, Maria G. Perrone, Carlo Franchini, Giovanni Lentini, Stereoselective Modulation of P-Glycoprotein by Chiral Small Molecules, ChemMedChem 11 (1) (2016) 93–101, https://doi.org/10.1002/cmdc.201500417.
[37] N.L. Urizar, A.B. Liverman, D.T. Dodds, F.V. Silva, P. Ordentlich, Y. Yan, F. J. Gonzales, R.A. Heyman, D.J. Mangelsdorf, D.D. Moore, A natural product that lowers cholesterol as an antagonist ligand for FXR, Science 296 (2002) 1703–1706, https://doi.org/10.1126/science.1072891.
[38] Jisong Cui, Li Huang, Annie Zhao, Jane-L. Lew, Jinghua Yu, Soumya Sahoo, Peter T. Meinke, Inmaculada Royo, Fernando Peláez, Samuel D. Wright, Guggulsterone is a farnesoid X receptor antagonist in coactivator association assays but acts to enhance transcription of bile salt export pump, J. Biol. Chem. 278 (12) (2003) 10214–10220, https://doi.org/10.1074/jbc.M209323200.